First-principles study of the effect of hydrogen on the metal–ceramic interface

2005 J. Phys.: Condens. Matter 17 5335

(http://iopscience.iop.org/0953-8984/17/35/002)

INSTITUTE OF PHYSICS PUBLISHING JOURNAL OF PHYSICS: CONDENSED MATTER

J. Phys.: Condens. Matter **17** (2005) 5335–5348 doi:10.1088/0953-8984/17/35/002

First-principles study of the effect of hydrogen on the metal–ceramic interface

L M Liu[1,2,4], **S Q Wang**[1] **and H Q Ye**[1,3]

[1] Shenyang National Laboratory for Materials Science, Institute of Metal Research, Chinese Academy of Sciences, Shenyang 110016, People's Republic of China
[2] Graduate School of Chinese Academy of Sciences, Beijing 100049, People's Republic of China
[3] Electron Microscope Lab, Peking University, Beijing 100871, People's Republic of China

E-mail: lmliu@imr.ac.cn

Received 24 April 2005, in final form 19 June 2005
Published 19 August 2005
Online at stacks.iop.org/JPhysCM/17/5335

Abstract

We employ density functional theory to investigate the effect of hydrogen on TiN(111) surfaces and Al/TiN(111) interfaces. The results show that hydrogen atoms prefer to sit over different sites when adsorbing on the N- and Ti-terminated TiN(111) surfaces. Subsequent study shows that the work of adhesion of the hydrogen contaminated TiN(111) interface is substantially lower than that of the clean surface. A thorough analysis of the atomic structure and electronic density shows that hydrogen atoms break the original strong interfacial Al–N or Al–Ti bond of the clean surface and the new interfacial Al–H bond is rather weak. To gain insight into the tensile strength of the hydrogen contaminated interface, the tensile process is fully simulated. The different fracture behaviours are revealed for the clean interface and the hydrogen contaminated one: the fracture of the clean interface is ductile inside the Al slab, while that of the hydrogen contaminated interface is at the interface. Our calculated work of adhesion and tensile strength are quantitatively consistent with available theoretical and experimental results.

(Some figures in this article are in colour only in the electronic version)

1. Introduction

Titanium nitride and carbide, due to owning excellent properties, are commonly used in wear- or corrosion-resistant coatings on mechanical components, electrical contacts, diffusion barriers in electronic devices and metal matrix composites [1–4]. The strength of a metal–ceramic interface is strongly influenced by the chemical composition of the region at or close to the interface. Both structure and bonding across the interface have great effects on the properties of

[4] Author to whom any correspondence should be addressed.

such materials. To design and optimize such metal–ceramic materials the first essential question is how to understand atomic structures and bonding mechanisms at the atomic level [5–7].

Titanium nitride films are usually produced by various chemical vapour deposition (CVD) techniques. The common nitriding components of the CVD procedure are NH_3, $H_2 + N_2$ and N_2H_4 [8–11]. To fabricate the microelectronic devices, Al is subsequently deposited on top of TiN film. Throughout the whole process hydrogen has the opportunity to adsorb on TiN surface, and then segregate to the Al/TiN interface. Hydrogen adsorption on the surface and segregation to the interface may substantially affect the surface and interfacial chemical bonding and result in a modification of the material properties.

Many first-principles density functional theory (DFT) calculations have been applied to metal–ceramic interfaces, but most of them [12–20] deal with metal–oxide interfaces. The metal–transition metal carbide or nitride interfaces have been studied [21–27], but they are not widely investigated theoretically. On the other hand, there are few studies on the effect of gases, such as hydrogen and oxygen, on the metal–ceramic interface. Wang *et al* [28] studied the effect of hydrogen on the Al_2O_3/Cu interfacial structure and adhesion, and they found that fracture would happen within the Cu slab, both with and without the presence of interfacial hydrogen. Łodziana and Nørskov [29] studied the adsorption of Cu and Pd on Al_2O_3 surfaces with different stoichiometries, and they concluded that stoichiometric hydroxylation of the surface did not increase the metal–oxide interaction significantly. Recently, Qi and Hector [30] found that hydrogen greatly decreased the adhesion of the Al/diamond interface and the hydrogen contaminated interface fractured easily.

Marlo and Milman have discussed the adsorption and diffusion of hydrogen on the nonpolar TiN(001) surface [31]. As far as we know, there has still been no theoretical research on the effect of gases on the metal/nitride (carbide) interface. The nitrides and carbides have quite different properties from the oxides and diamond, so gases may have completely different effects on the nitrides and carbides from other compounds.

Experimentally, both the Al/TiN(001) and Al/TiN(111) have been widely fabricated [10, 11]. In an earlier study [32], the optimal atomic structure, work of adhesion, electronic properties and stability of the polar Al/TiN(111) interfaces have been thoroughly examined. Continuing this study, one main purpose of this work is to investigate the preference site, adsorption energy and electronic properties of hydrogen adsorption on the differently terminated TiN(111) surfaces. A further purpose is to explore the effect of hydrogen on the interfacial structure, adhesion, tensile strength and electronic properties.

The remainder of this paper is organized as follows. Section 2 describes the computational methodology used in this study. Section 3 mainly exhibits the properties of hydrogen adsorption on the polar TiN(111) surface. The major results of this paper are presented in section 4, where we discuss the properties of adhesion energies, electronic structures and tensile strengths of the clean interface and the hydrogen contaminated one. Finally, we summarize our results in section 5.

2. Methodology

We use the CASTEP [33] package in our calculations; it is based on density functional theory [34, 35], and uses a plane-wave basis set for the expansion of the single-particle Kohn–Sham wavefunctions and Vanderbilt ultrasoft pseudopotentials (US PP) [36] to describe the ionic cores. The exchange–correlation energy is described by the generalized gradient approximation of Perdew and Wang (GGA-PW91) [37]. Electronic relaxation was performed using the Pulay density mixing along with the conjugate gradient minimization method. A Fermi function is used with a temperature broadening parameter of 0.1 eV to improve the

Table 1. Calculated values of the lattice constants a_0, bulk modulus B and cohesive energies E_{coh} of the bulk Al and TiN compared with other calculations and experimental (expt) data.

System	Method	a (Å)	B (Mbar)	E_{coh} (eV)
TiN	This work	4.24	2.70	6.88
	GGA-PWPP[a]	4.25	2.78	6.80
	GGA-FP-LMTO[b]	4.23	2.70	—
	Expt	4.238[c]	2.88[d]	6.69[e]
Al	This work	4.02	0.75	3.46
	GGA-PWPP[a]	4.05	0.75	3.45
—	GGA-LAPW[f]	4.05	0.73	—
	Expt	4.05[g]	0.79[h]	3.39[g]

[a] Reference [39].
[b] Reference [40].
[c] Reference [41].
[d] Reference [42].
[e] Reference [43].
[f] Reference [44].
[g] Reference [45].
[h] Reference [46].

convergence. Ground state atomic geometries are determined by minimizing the Hellmann–Feynman forces. Ionic relaxation was performed using the Broyden–Fletcher–Goldfarb–Shanno (BFGS) update scheme, until the root mean square forces on the atoms were less than 0.05 eV Å^{-1}. The Brillouin zone is sampled with a Monkhorst–Pack k-point grid [38]. For the bulk an $[8 \times 8 \times 8]$ k-point mesh is used and for the slab an $[8 \times 8 \times 1]$ k-point mesh is used. The plane-wave cut-off in our calculations is 350 eV. This set of parameters ensures a total energy convergence of 0.01 eV per atom.

3. Bulk and surface calculations

3.1. Bulk properties

To assess the accuracy of our computation method, in particular that of the pseudopotentials used, we performed a series of calculations on the structural properties of TiN, Al and H_2.

Table 1 shows our results for the lattice constants, bulk moduli and cohesive energies of Al and TiN, compared with other theoretical and experimental values. For TiN, our calculated result for the lattice constant (4.24 Å) is in good agreement with the experimental result (4.238 Å) [41]. The bulk modulus underestimates the experimental result by 6.3%, and it is in excellent agreement with other full-potential linear muffin-tin orbital (FP-LMTO) results. For Al, the calculated result for the lattice constant (4.02 Å) underestimates the experimental result. The bulk modulus is in agreement with the experimental result. For both TiN and Al, the results for cohesive energies agree well with the experimental values.

For the hydrogen molecule, the calculated bond length is 0.752 Å, which is in excellent agreement with the experimental result (0.766 Å). Meanwhile, the cohesive energy (2.27 eV/atom) is slightly larger than another calculated result, 2.23 eV/atom [47].

In all, our calculated results for TiN, Al and H_2 are in good agreement with available experimental and other calculated results, thereby validating the application of the methodology for studying the surface and interfacial properties.

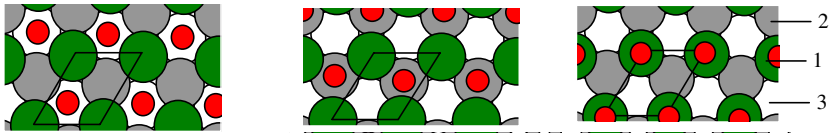

Figure 1. Three high symmetry sites for both terminations: (a) FCC, (b) HCP, (c) OT. The small spheres present the hydrogen atoms; the large spheres denote the Ti or N atoms of TiN. Layers 1, 2 and 3 indicate the surface, sub-surface and third-layer atoms of the TiN, respectively.

Table 2. Calculated adsorption energy (E_{ads}) and the separation distance (d_0) between the hydrogen atom and the surface layer for the N-terminated and Ti-terminated TiN(111) surfaces.

Systems	Layers	Stacking	d_0 (Å)	W_{ads} (eV)
N termination	7	FCC	0.30	0.72
		HCP	0.67	0.60
		OT	1.02	3.11
	9	FCC	0.30	0.71
		HCP	0.67	0.60
		OT	1.02	3.11
Ti termination	7	FCC	0.97	3.59
		HCP	1.13	3.25
		OT	1.73	1.93
	9	FCC	0.99	3.55
		HCP	1.12	3.22
		OT	1.73	1.97

3.2. Adsorption of hydrogen on the TiN(111) surface

During the process of fabricating the TiN film by CVD, hydrogen may adsorb on the polar TiN(111) surface. To establish the possibility of the hydrogen atom adsorbing and the preferred site, we consider three different sites, placing the hydrogen atom in one of three high symmetry positions with respect to the ceramic surface lattice structure (illustrated in figure 1).

The adsorption energy, E_{ads}, is calculated as the energy difference

$$E_{ads} = E_{TiN} + E_H - E_{H/TiN} \tag{1}$$

where E_{TiN}, E_H and $E_{H/TiN}$ are the total energy of the TiN(111) slab, the hydrogen atom and the hydrogen contaminated TiN(111) slab, respectively. To make sure that the TiN(111) slab is thick enough for simulating the surface, we test both seven-layer and nine-layer slabs of TiN(111). The results for the adsorption energy and structure parameter are shown in table 2. It is obvious that the adsorption energies and structure parameters of the seven-layer and nine-layer slabs for any site show little difference, especially for the N-terminated surface. So a seven-layer slab is thick enough for simulating the TiN(111) surface.

The differently terminated surfaces show nearly opposite characters when hydrogen atoms adsorb on the N- and Ti-terminated TiN(111) surfaces. For the N-terminated surface, hydrogen atoms prefer to adsorb over the OT site. The hydrogen atom is at a small distance, 1.02 Å, from the N-terminated surface. The adsorption energy of the OT site is 3.11 eV. For the FCC site, the hydrogen atom is at a very small distance, only 0.30 Å, from the N-terminated surface. But the adsorption energy of the FCC site is only 0.72 eV.

For the Ti-terminated TiN(111) surface, however, the FCC site is the most energetically optimal site of the three. The adsorption energy of the HCP site is rather close to that of the FCC site. The OT site is the most unfavourable one of the three. The adsorption energy of the FCC site is 3.59 eV, which is larger than that of the most preferred site (OT) for the N-terminated case.

Further, for the Ti-terminated surface the adsorption energy is inversely proportional to the separation distance between the hydrogen atom and the surface layer. With increase of the separation distance, the adsorption energy substantially decreases. For the FCC site the distance is 0.97 Å and the corresponding adsorption energy is 3.59 eV. For the OT site the distance becomes 1.73 Å, and the adsorption energy reduces to 1.93 eV. But for the N-terminated TiN(111) surface there is no such relation between the separation distance and the adsorption energy.

To clarify the intrinsic mechanism, the interaction between the hydrogen atom and TiN(111) surface for the optimal structure of each terminated surface is analysed using the layer-projected density of states (LDOS). Figure 2 shows the LDOS projected onto the clean TiN(111) and the hydrogen contaminated N-terminated (H:N–TiN(111)) and Ti-terminated (H:Ti–TiN(111)) surfaces.

For the N-terminated surface, both the surface N layer and the sub-layer (the layer nearest to the surface) of the clean TiN(111) surface show more states near the Fermi level. This is consistent with our previous finding that the N-terminated surface has relatively large relaxation and surface energy [32]. The hydrogen adsorption on such a surface changes not only the states of the surface N layer, but also those of the sub-surface Ti layer. The main feature is that there are significant H 1s and N 2sp orbital mixings from -16 to -14 eV and from -8 to -6 eV. Meanwhile, the states of the surface N layer have been substantially redistributed and the original high energy states have been moved to more stable low energy states compared with those of the clean surface.

For the Ti-terminated surface, the effect of hydrogen adsorption is mainly confined to the surface Ti layer; there is little change at the sub-layer. The overlapping states of the surface Ti 3d and H 1s are mainly from -8 to -3 eV. The original peak of the surface Ti layer has been greatly depleted at the Fermi level compared with that of the clean surface, which results from the charge transfer from Ti to H atoms. Further, the states of the hydrogen atom from -8 to -3 eV are obviously larger than those for the corresponding N-terminated surface. That is to say, the H:Ti–TiN(111) surface has more charge transfer from the surface layer to the hydrogen atom than the H:N–TiN(111) one. This could be the main reason for hydrogen atom adsorption on the Ti-terminated surface having a slightly larger adsorption energy.

In summary, we find that hydrogen atoms prefer different sites when adsorbing on the differently terminated surfaces. A thorough analysis of bonding shows that the H:Ti–TiN(111) surface has a slightly larger adsorption energy than the H:N–TiN(111) one because the H:Ti–TiN(111) surface has more charge transfer from the surface layer to the hydrogen atom.

4. Interfaces

4.1. Model geometry

In our previous study, we found that the metal Al, keeping the stacking sequence of the ceramic across the interface, has the largest work of adhesion [32]. In this study, we will concentrate on this most optimal structure and clarify the effect of hydrogen on the interface. Our interfacial model uses a superlattice geometry in which a five-layer Al(111) slab is placed on a nine-layer clean or hydrogen contaminated TiN(111) slab with different interfacial distance, and then the

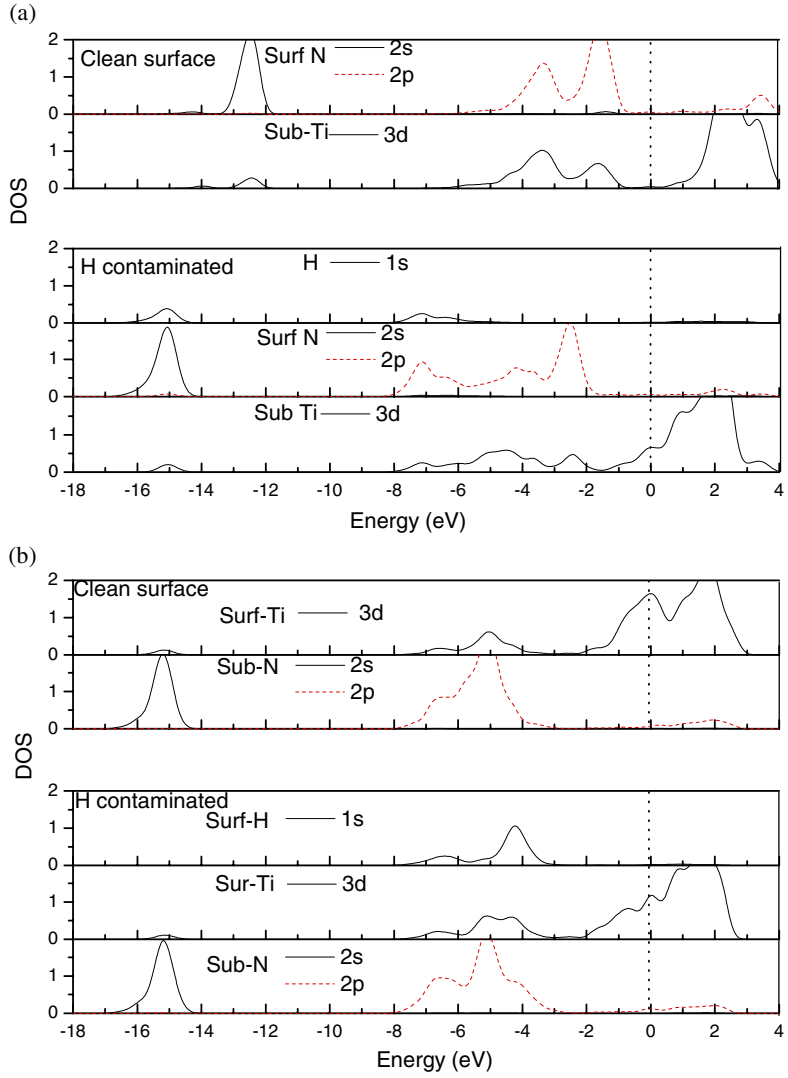

Figure 2. Layer-projected DOS for the surface and sub-layer of the clean TiN(111) surface and hydrogen contaminated TiN(111) surface: (a) N-terminated and (b) Ti-terminated cases. The upper panel is for the clean surface and the lower panel is for the hydrogen contaminated one. The vertical dotted line gives the location of the Fermi level.

atomic coordinates are relaxed. The most optimal structure is the one that shows the minimum energy. There are in total 14 atoms for the clean interfaces and 16 atoms for the hydrogen contaminated ones. There is no vacuum between the slabs. To avoid a dipole moment, inverse symmetry is used.

4.2. Work of adhesion

The ideal work of adhesion, W_{ad}, an important fundamental quantity for predicting the mechanical properties, is defined as the reversible work needed to separate an interface into

Table 3. Calculated relaxed work of adhesion (W_{ad}) and the interfacial separation (d_0) for the clean and hydrogen contaminated interface systems.

Systems	d_0 (Å)	W_{ad} (J m^{-2})
N termination	0.93	4.28
	0.98	3.98[a]
N termination:H	2.6	0.33
Ti termination	2.18	3.84
	2.29	3.59[a]
Ti termination:H	1.77	0.98

[a] Reference [32].

two free surfaces. W_{ad} can be given by the difference in total energy between the interface and its isolated slabs:

$$W_{ad} = (E_A^{tot} + E_B^{tot} - E_{A/B}^{tot})/2A. \quad (2)$$

Here, E_A^{tot} and E_B^{tot} are the total energies of the relaxed, isolated clean TiN or hydrogen contaminated TiN and Al slabs in the same supercell when one of the slabs is retained and the other one is replaced by vacuum, respectively, and $E_{A/B}^{tot}$ is the total energy of the clean or hydrogen contaminated interface system. A is the interface area of the unit cell. Generally, the mechanical work needed to separate at an interface is larger than the ideal work of adhesion, W_{ad}, due to the neglect of plastic and diffusional degrees of freedom, as discussed by Finnis [5]. As regards the effect of impurity on the work of adhesion, Zhang and Smith revealed that the position of the impurities after separation greatly affects the work of adhesion [56]. In our later tensile test, we showed that the weakest part of the interface is between the Al and H atoms. In this study, we only examined the lowest work of adhesion.

Our calculated results for the optimal interfacial separation (d_0) and work of adhesion (W_{ad}) are shown in table 3. For the clean interface, our results are compared with previous results. The W_{ad} from this method for each termination is a little larger than that from the previous vacuum model. One main reason may be that the lattice constant of Al underestimates the experimental result, which makes the lattice mismatch (6.6%) a little larger than that for the previous method (4.8%). The relatively large lattice mismatch usually leads to overestimation of the work of adhesion, as discussed in [48, 49].

For each termination, the work of adhesion for the hydrogen contaminated interface is significantly lower than that for the corresponding clean one. For the Al/H:N–TiN interface, the W_{ad} is weakened from 4.28 J m^{-2} (the clean case) to 0.33 J m^{-2}. Meanwhile the interfacial separation is also greatly enlarged. For the Al/H:Ti–TiN interface, the W_{ad} is a little higher, 0.98 J m^{-2}, than that for the Al/H:N–TiN one, but it is also substantially lower than that for the clean interface (3.84 J m^{-2}). This is quantitatively in agreement with other results for Al/H:C-1 $\times$ 1, which showed that W_{ad} was reduced from 3.98 to 0.02 J m^{-2} [30].

To gain insight into the cause, the LDOS is explored to study the interfacial electronic structure and bonding. The results for the clean interface and the hydrogen contaminated one are shown in figure 3.

First, we start by investigating the N-terminated interface (figure 3(a)). For the clean Al/TiN(111) interface, there are a series of low energy Al 3sp–N 2sp overlapping orbitals, which contribute to the formation of the strong polar bond. But for the hydrogen contaminated interface, the Al–N bond has been completely broken. The original overlapping N 2s and Al 3sp states from -17 to -15 eV completely disappear. The LDOS of the interfacial Al shows some electronic states at the Fermi level and looks like the free electronic one. There are very

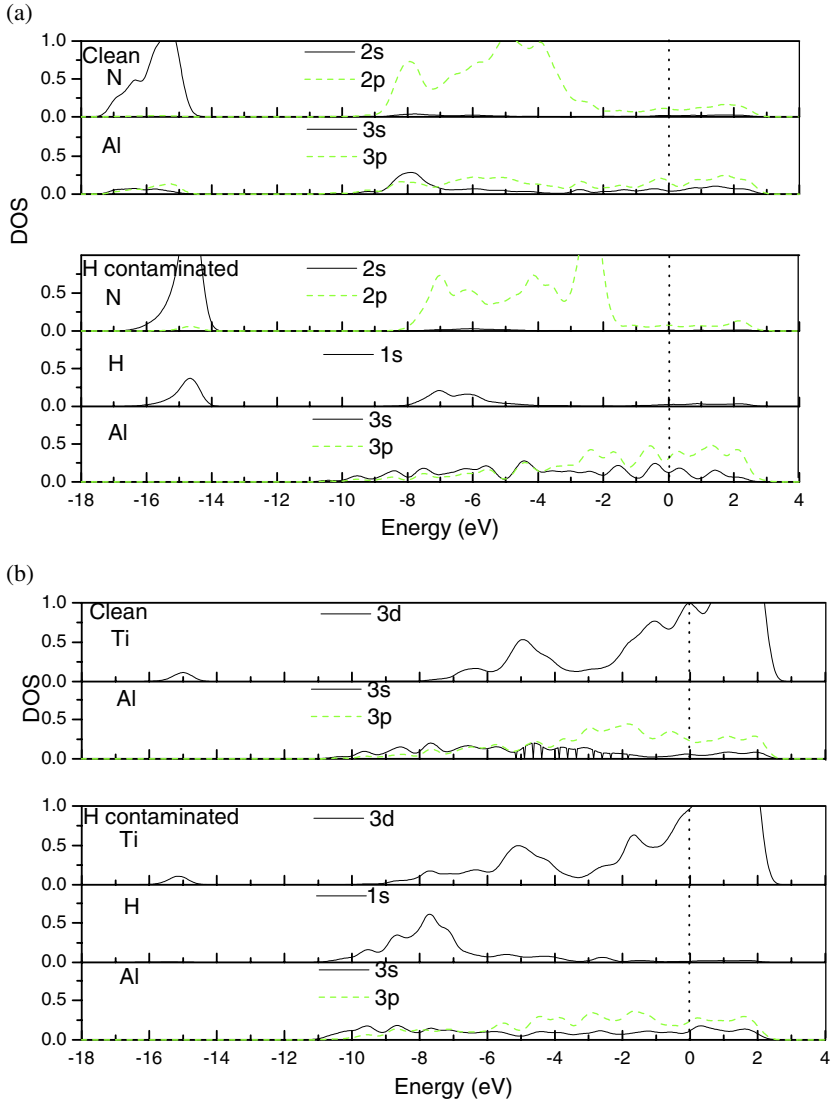

Figure 3. Layer-projected DOS for the (a) N-terminated (b) Ti-terminated interface structures. The upper panel is for the clean surface and the lower panel is for the hydrogen contaminated one. The vertical dotted line gives the location of the Fermi level.

few H 1s and Al 3sp overlapping states, which is why the hydrogen contaminated interface exhibits a very low work of adhesion.

Next, we turn to considering the Ti-terminated interface (figure 3(b)). For the clean interface, the interactions of Al and Ti are mainly metallic bonding, as found in our previous study. For the hydrogen contaminated interface, the orbital H 1s and Al 3sp interactions are mainly from −10 to −6 eV. Compared with the case of the hydrogen contaminated surface (figure 2(b)), the interfacial hydrogen atom shows rather stronger peaks from −10 to −6 eV, which is a result of charge transfer from the interfacial Al slab to the hydrogen atom. For the N-terminated interface such phenomena of charge transfer are not observed. So this explains well why the Al/H:Ti–TiN interface is a little stronger than the Al/H:N–TiN interface.

In all, hydrogen is rather a disadvantage to the Al/TiN(111) interface. For each termination, hydrogen deceases the work of adhesion substantially. The electronic analysis shows that the original strong Al 3sp–N 2sp or Al 3sp–Ti 3d bond of the clean interface is completely broken by hydrogen atoms and the new Al 3sp–H 1s bond is rather weak, especially for the Al/H:N–TiN(111) case.

4.3. Tensile test

To estimate the strength of the clean interface and the hydrogen contaminated one, a tensile test simulation is examined. In the tensile test, uniaxial strain is introduced into the supercell of the stable configurations [50–53]. First, the tensile test is simulated by gradually increasing the dimension in the z-direction. The atomic positions of the whole systems are increased according to the new dimension in the z-direction, and then the atomic positions of the new configuration are fully relaxed at each stage of strain. The next initial strain configuration will start from the relaxed configuration. The procedure continues until the interface is completely broken. This process mimics a real tensile test at zero temperature.

4.3.1. Tensile process. To gain insight into the fracture processes of the different interfaces, we plotted the relaxed atomic configuration and the electronic density at each strain level for all interfaces, as shown in figure 4. Most importantly, there are significantly different behaviours of the clean interface and the hydrogen contaminated one. The fracture of the clean interface happens at the second layer of the Al slab due to the strong bonding at the interface, while the fracture of the hydrogen contaminated one happens easily at the interface.

Further, the fracture processes for the two terminations show some different behaviours. First, for the clean interfaces the two terminations show nearly similar fracture characters (figures 4(a) and (c)). At the initial stage (strain 0%), there is a large amount of charge accumulation at the interface. With the increase of the strain, a charge density void appears at the sub-layer of the Al slab. The configuration of the depletion region is at first a small circle, and then the small circle gradually grows bigger. When the strain reaches 15%, the circle extends into a long band parallel to the interface. Then the band expands quickly normal to the interface until the Al slab fractures.

Second, the two hydrogen contaminated interfaces have different fracture processes. For the Al/H:N–TiN(111) interface (figure 4(b)), there is evidently little electronic accumulation between the Al and H atoms. There is a large band of depletion region existing parallel to the interface even at the strain of 0%. With the strain increasing, the band extends quickly normal to the interface. The fracture happens easily due to the weak bonding between the Al and H atoms, while for the Al/H:Ti–TiN(111) case (figure 4(d)) there is some electronic accumulation between the Al and H atoms at the strain of 0%, consistent with the above analysis of the LDOS. An electronic depletion zone emerges at the strain of 5%, and the electronic depletion zone soon enlarges into a long band at the strain of 10%. After this stage the band expands quickly normal to the interface and the interaction between the interfacial H and Al atoms is soon cleaved.

It is obvious that the fracture processes of all these interfaces can be separated into two groups: one is for the clean Al/TiN(111) interface and the Al/H:Ti–TiN(111) one, and the other is for the Al/H:N–TiN(111) interface. For the first group, the fracture process experiences two stages. In the first stage, a charge density void appears and then expands into a band parallel to the interface. In the second stage, the band extends normal to the interface until the material fractures. When the fracture process of the second group does not experience the first stage the void expands along the interface and only in the second stage the void extends normal to the interface.

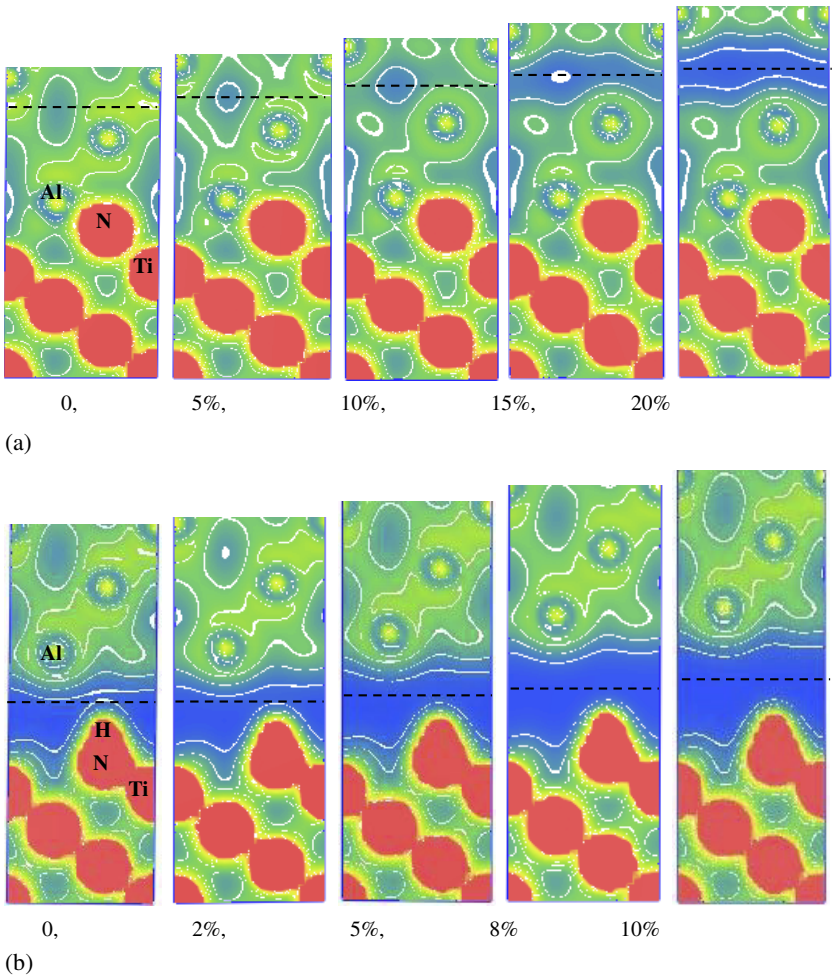

Figure 4. Relaxed atomic configuration and contours of the electronic density at each strain level for the (a) Al/N–TiN, (b) Al/H:N–TiN, (c) Al/Ti–TiN, (d) Al/H:Ti–TiN interfaces. Only half of the supercell is shown for each interface. The strain is labelled below each picture. The parallel dotted line gives the location of the fracture.

4.3.2. Tensile strength. The tensile stress as a function of tensile strain is shown in figure 5. The clean interface and the hydrogen contaminated one show completely different behaviours, as found above. First, we discuss the clean Al/TiN interface. For the clean Al/TiN(111) interface, each termination experiences an elastic deformation at the first stage. The two interfaces have maximum stress at nearly the same strain (about 10%). The maximum stress of the Ti-terminated interface is 13.22 GPa, which is the upper bound of the tensile strength. This value is a little larger than that of the N-terminated case (12.15 GPa). After reaching its maximum value at the strain of 10%, the tensile stress decreases rapidly. We note that the theoretical tensile strength of an Al single crystal is 11.05 GPa [54]. Although fracture of the metal/nitride material also happens within the Al slab, the strength value is higher than that for the pure Al. The main reason results from the strong interaction interface, which can transfer some stress to the ceramic side. Further, we note that the experimental result for the TiC/Al strength is 9.25 GPa [55], which is fairly comparable with our result.

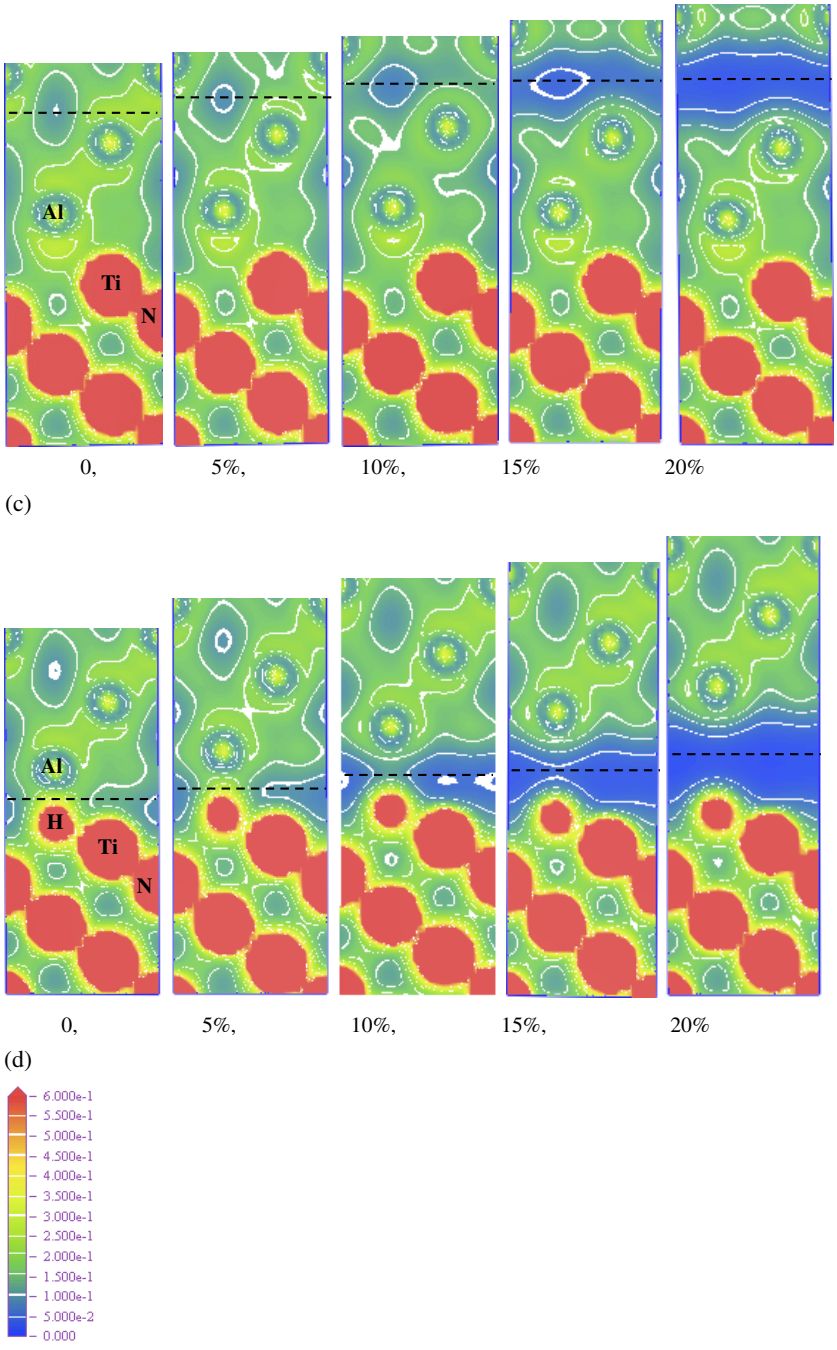

Figure 4. (Continued.)

It seems contradictory that the clean N-terminated interface has a larger work of adhesion but a lower tensile strength than the clean Ti-terminated one. In fact, for the clean interfaces, the interfacial bonding for both terminations is strong, as evidenced by the large values for

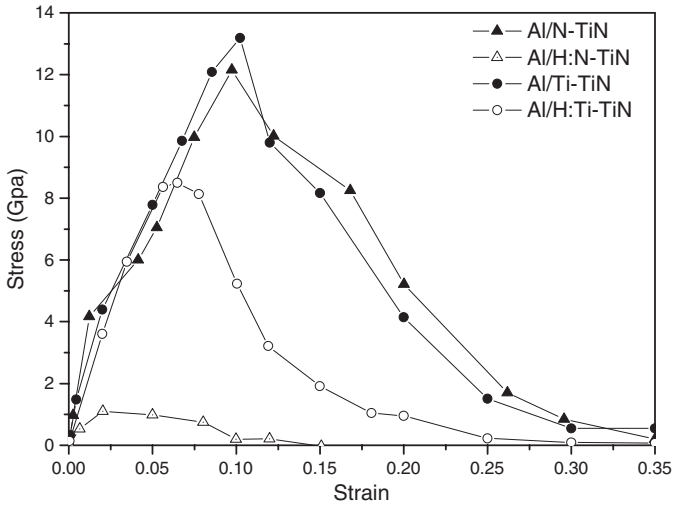

Figure 5. The tensile stress as a function of the tensile strain during the tensile test.

W_{ad}. Cleavage therefore occurs in the Al slab. Under these circumstances, one would expect the interface to have little effect on the tensile strength. This is confirmed by figure 5, where the tensile strengths are similar. The reason that the N-terminated interface, despite having a larger W_{ad}, has a smaller tensile strength (relative to Ti-terminated one) is the charge transfer to the interfacial N atoms. This would decrease the bonding between Al(111) layers.

Next, let us concentrate on the hydrogen contaminated interface. Most importantly, the Al/H:N–TiN(111) interface does not experience any elastic deformation stage, as found in the tensile process, and the maximum stress is only 1.1 GPa at the strain of 2%. The Al/H:Ti–TiN(111) one experiences a short elastic deformation stage and the maximum stress is 8.36 GPa at the strain of 6.2%. Though the maximum stress of the Al/H:Ti–TiN(111) interface is obviously lower than that of the clean one, it is nearly eight times that in the Al/H:N–TiN(111) case.

5. Summary and conclusions

We have performed a first-principles study of the work of adhesion, atomic and electronic structure, and tensile strength of hydrogen contaminated TiN(111) surfaces and Al/TiN(111) interfaces compared with those for the clean ones in order to understand how hydrogen affects the properties of the metal/nitride material.

The preferred site and adsorption energy for hydrogen adsorption on the TiN(111) surface have been thoroughly investigated. The results show that hydrogen atoms prefer different sites when they adsorb on the differently terminated TiN(111) surfaces. For the N-terminated TiN(111) surface, the hydrogen atom prefers to sit directly over the surface nitrogen atom, while for the Ti-terminated TiN(111) surface the hydrogen atom chooses to sit over the FCC hollow site. The subsequent LDOS shows that there is a bigger charge transfer from the Ti-terminated surface layer to the hydrogen atom than from the N-terminated one. This is the main reason that the former has a larger adsorption energy than the latter.

Further, the effect of hydrogen on the work of adhesion is examined. For the N-terminated interface, hydrogen decreases the work of adhesion from 4.28 J m^{-2} for the clean case to

0.33 J m^{-2}. For the Ti-terminated interface, hydrogen reduces the work of adhesion from 3.84 J m^{-2} for the clean case to 0.98 J m^{-2}. So hydrogen decreases the work of adhesion of the N-terminated interface more than that of the Ti-terminated one. Thorough analysis of the atomic and electronic structure reveals the intrinsic mechanism. For the N-terminated interface, the original strong Al 3sp–N 2sp bond has been completely broken, and there is nearly no interaction between the Al 3sp and H 1s. For the Ti-terminated interface, the Al–Ti bonding is also broken, but there is some interaction between the H 1s and Ti 3d.

Lastly, the effect of hydrogen on the tensile strength has been tested. The electronic density shows that the fracture processes for the clean Al/TiN(111) interface and the Al/H:Ti–TiN(111) one are quite different. For the clean interface, the fracture happens within the softer Al side and the fracture process has an elastic deformation stage. For the hydrogen contaminated interface, the fracture occurs at the interface. Hydrogen greatly decreases the tensile strength: (i) for the Al/H:Ti–TiN interface, hydrogen shortens the elastic deformation stage; (ii) for the Al/H:N–TiN interface, hydrogen eliminates the elastic deformation stage, so the tensile strength is rather low. The calculated results for the tensile strength are quantitatively in agreement with available calculated and experimental results.

Acknowledgment

This work was supported by the Special Funds for Major State Basic Research Projects of China (No G2000067104).

References

[1] Johansson L I 1995 *Surf. Sci. Rep.* **21** 177
[2] Xiao P and Debry B 1996 *Acta. Mater.* **44** 307
[3] Frumin N, Frage N, Polak M and Dariel M P 1997 *Scr. Mater.* **37** 1263
[4] Hultman L 2000 *Vacuum* **57** 1
[5] Finnis M W 1996 *J. Phys.: Condens. Matter* **8** 5811
[6] Christensen A, Jarvis E A and Carter E A 2001 *Chemical Dynamic in Extreme Environment* ed R A Dreeler (Singapore: World Scientific)
[7] Sinnott S B and Dickey E C 2003 *Mater. Sci. Eng.* R **43** 1
[8] Choy K L 2003 *Prog. Mater. Sci.* **48** 57
[9] Hedge R I, Fiordalice R W, Travis E O and Tobin P J 1993 *J. Vac. Sci. Technol.* B **11** 1287
[10] Avinun A, Barel N, Kaplan W D, Eizenberg M, Naik M, Guo T, Chen L Y, Mosely R, Littau K, Zhou S and Chen L 1998 *Thin Solid Films* **320** 67
[11] Chun J-S, Desjardins P, Lavoie C, Shin C-S, Cabral C Jr, Petrov I and Greene J E 2001 *J. Appl. Phys.* **89** 7841
[12] Li C, Wu R Q, Freeman A J and Fu C L 1993 *Phys. Rev.* B **48** 8317
[13] Christensen A and Carter E A 2000 *Phys. Rev.* B **62** 16968
[14] Batyrev I G, Alavi A and Finnis M W 2000 *Phys. Rev.* B **62** 4698
[15] Jarvis E A and Carter E A 2002 *Phys. Rev.* B **66** 100103
[16] Zhang W, Smith J R and Evans A G 2002 *Acta. Mater.* **50** 3803
[17] Wang X G, Smith J R and Evans A G 2002 *Phys. Rev. Lett.* **89** 286102
[18] Siegel D J, Hector L G Jr and Adams J B 2002 *Phys. Rev.* B **65** 085415
[19] Bogicevic A and Jennison D R 1999 *Phys. Rev. Lett.* **82** 799
[20] Zhukovskii Y F, Kotomin E A, Jacobs P W M and Stoneham A M 2000 *Phys. Rev. Lett.* **84** 1256
[21] Dudiy S V, Hartford J and Lundqvist B I 2000 *Phys. Rev. Lett.* **85** 1898
[22] Dudiy S V and Lundqvist B I 2001 *Phys. Rev.* B **64** 045403
[23] Siegel D J, Hector L G Jr and Adams J B 2002 *Acta. Mater.* **50** 619
[24] Siegel D J, Hector L G Jr and Adams J B 2003 *Phys. Rev.* B **67** 092105
[25] Kohyama M and Hoekstra J 2000 *Phys. Rev.* B **61** 2672
[26] Liu L M, Wang S Q and Ye H Q 2004 *Surf. Sci.* **550** 46
[27] Liu L M, Wang S Q and Ye H Q 2004 *J. Phys.: Condens. Matter* **16** 5781

[28] Wang X G, Smith J R and Scheffler M 2002 *Phys. Rev.* B **66** 073411
[29] Łodziana Z and Nørskov J K 2001 *J. Chem. Phys.* **115** 11261
[30] Qi Y and Hector L G Jr 2004 *Phys. Rev.* B **69** 235401
[31] Marlo M and Milman V 2000 *Phys. Rev.* B **62** 2899
[32] Liu L M, Wang S Q and Ye H Q 2004 *Acta. Mater.* **52** 3681
[33] Payne M C, Teter M P, Allan D C, Arias T A and Joannopoulos J D 1992 *Rev. Mod. Phys.* **64** 1045
[34] Hohenberg P and Kohn W 1964 *Phys. Rev.* **136** B864
[35] Kohn W and Sham L J 1965 *Phys. Rev.* **140** A1133
[36] Vanderbilt D 1990 *Phys. Rev.* B **41** 7892
[37] Perdew J P, Chevary J A, Vosko S H, Jackson K A, Pederson M A, Singh D J and Fiolhais C 1992 *Phys. Rev.* B **46** 6671
[38] Monkhorst H J and Pack J D 1976 *Phys. Rev.* B **13** 5188
[39] Liu L M, Wang S Q and Ye H Q 2003 *J. Phys.: Condens. Matter* **15** 8103
[40] Ahuja R, Eriksson O, Wills J M and Johansson B 1996 *Phys. Rev.* B **53** 3072
[41] Schoenberg N 1954 *Acta Chem. Scand.* **8** 213
[42] Gubanov V A, Ivanovsky A L and Zhukov V P 1994 *Electronic Structure of Refractory Carbides and Nitrides* (Cambridge: Cambridge University Press)
[43] Häglund J, Grimvall G, Jarlborg T and Guillermet A F 1991 *Phys. Rev.* B **43** 14400
[44] Asato M, Settels A, Hoshino T, Asada T, Blügel S, Zeller R and Dederichs P H 1999 *Phys. Rev.* B **60** 5202
[45] Kittel C 1996 *Introduction to Solid State Physics* 7th edn (New York: Wiley)
[46] Kamm G N and Alerts G A 1964 *J. Appl. Phys.* **35** 1257
[47] Michaelides A and Hu P 2000 *J. Chem. Phys.* **112** 6006
[48] Hong T, Smith J R and Srolovitz D J 1995 *Acta. Metall. Mater.* **43** 2721
[49] Schnitker J and Srolovitz D J 1998 *Modelling Simul. Mater. Sci. Eng.* **6** 153
[50] Kohyama M 2002 *Phys. Rev.* B **65** 184107
[51] Jhi S-H, Louie S G, Cohen M L and Morries J W Jr 2001 *Phys. Rev. Lett.* **87** 075503
[52] Roundy D and Cohen M L 2001 *Phys. Rev.* B **64** 212103
[53] Lu G, Orlikowski D, Park I, Politano O and Kaxiras E 2002 *Phys. Rev.* B **65** 64102
[54] Li W and Wang T 1999 *Phys. Rev.* B **59** 3993
[55] Katipellic L R, Agarwal A and Dahotre N B 2000 *Mater. Sci. Eng.* A **289** 34
[56] Zhang W and Smith J R 1999 *Phys. Rev. Lett.* **82** 3105